Auger and x-ray photoemission spectroscopy study on Cs_2Te photocathodes

A. di Bona[a] and F. Sabary
Commissariat à l'Energie Atomique, Centre d'Etudes de Bruyères-le-Châtel, B.P. 12, 91680 Bruyères-le-Châtel, France

S. Valeri
Istituto Nazionale di Fisica della Materia and Dipartimento di Fisica di Modena, Via G. Campi 213/a, 41100 Modena, Italy

P. Michelato and D. Sertore
Istituto Nazionale di Fisica Nucleare, Laboratorio LASA, Via fratelli Cervi 201, 20090 Segrate (MI), Italy

G. Suberlucq
CERN–Division PS, Group LP, CH-1211, Geneva 23, Switzerland

(Received 22 March 1996; accepted for publication 22 May 1996)

Thin films of Cs_2Te have been produced and analyzed by Auger depth profiling and x-ray photoemission spectroscopy (XPS). The formation of the photoemissive material passes through different phases, each of them has been characterized by XPS and by its total yield in the spectral region 3.5–5 eV. Copper and molybdenum substrates have been considered. While Mo behaves to all practical purposes like an ideal support for Cs_2Te, strong diffusion from the substrate material into the photoemissive film has been observed on photocathodes fabricated on Cu. The ruggedness of the photocathodes has been tested by exposing them to a few hundred Langmuirs of different gases, namely O_2, CO_2, CO, N_2, and CH_4. The last three have no effect on the photocathode lifetime, while a substantial reduction of the quantum efficiency has been observed after the exposure to oxygen. The main reason for this is the formation of a thick cesium oxide layer at the surface of the photocathode. However, the oxygen pollution can be partially recovered by the combined effect of heating the photocathode at 230 °C and illuminating the poisoned material with the 4.9 eV radiation. No rejuvenation has been observed under the effect of the temperature or the radiation alone. [S0021-8979(96)00517-8]

I. INTRODUCTION

For many years, the practical applications of Cs_2Te photocathodes was limited to solar blind light detectors[1] and reference standards for ultraviolet (uv) light intensity.[2] Very recently, the interest in this material has been renewed due to the application they could have in high quality electron sources for particle accelerators.[3,4] Their operational lifetime in the radio frequency cavities is 20–30 times longer than that of (multi)alkali antimonide photocathodes,[5–8] making Cs_2Te the ''ideal'' photoemitter for laser-driven photoinjectors. The price we must pay for this, is the relatively high threshold energy (3.6 eV), which forces us to use uv radiation to produce the electron emission.

The optimization of this kind of electron source requires expertise that spans over a wide field of interests (accelerator technology, laser technology, materials science, surface analysis, and theoretical modeling), which can hardly be found in a single research center. Therefore, we coordinated the specific competencies of our laboratories in order to face the complexity of the problem from a general point of view. Despite the differences in the experimental systems, we were able to reproduce the main features of the Cs_2Te photocathodes (spectral response, lifetime, rejuvenation) in the various laboratories, pointing out that the set of experimental parameters we took into account, is large enough to ensure predictable results.

Even though the physical parameters that control the quantum efficiency have been known for over fifty years, the improvement of a particular material is usually attained by changing the fabrication parameters (by a combination of ''intelligent guessing'' and luck) in feedback with the photocurrent yield alone. Not much information can actually be gained about the processes that lead to the photoemissive material. An understanding of these processes may be useful for improving the reproducibility and the quantum efficiency of the photocathodes. To this purpose, a Cs_2Te preparation system has been connected, by a ultrahigh vacuum (UHV) transfer system to an analysis chamber, equipped with standard surface science facilities [scanning Auger, Ar^+ depth profiling, x-ray photoemission spectroscopy (XPS)]. With this experimental setup, the changes in the quantum yield can be directly correlated to the electronic structure of the material, which in turn give us much more information than the photocurrent alone.

II. EXPERIMENTAL TECHNIQUES

Cs_2Te thin films (tens of nanometers thick) were fabricated under UHV conditions (base pressure less than 5×10^{-11} mbar) onto metal substrates ($10\times10\times1$ mm high purity Mo and Cu foils). Before the introduction in the fabrication system, the substrates were mechanically polished

[a]Electronic mail: dibona@unimo.it

 0021-8979/96/80(5)/3024/7/$10.00

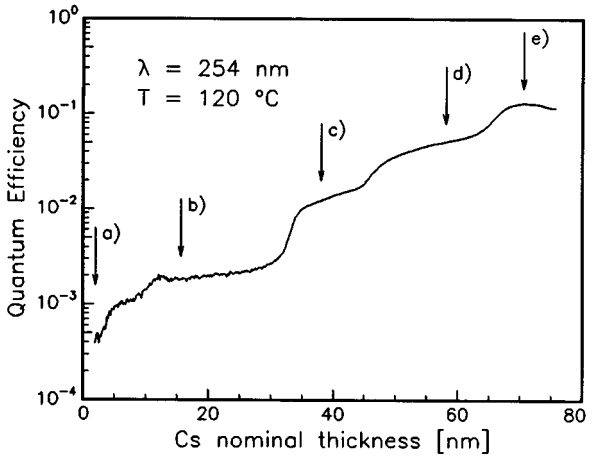

FIG. 1. Quantum efficiency as a function of the Cs nominal thickness during the fabrication of the photocathode. The substrate temperature is held at 120 °C. The arrows indicate the fabrication steps at which XPS experiments have been performed.

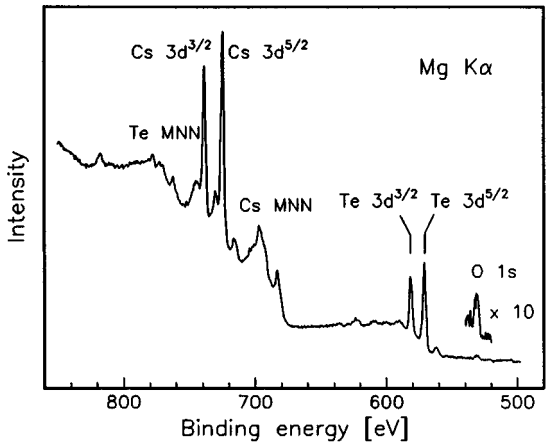

FIG. 2. Wide range XPS spectrum from the completed photocathode [step (e) of Fig. 1] at near-normal collection geometry.

with 1 μm diamond powder, then rinsed with acetone and ethanol. Once UHV conditions were obtained, the substrates were heated at 500 °C for about 30 min to improve the surface cleaning. During this phase, the total pressure never exceeded 2×10^{-9} mbar.

Te and Cs sources are Ni boats from SAES-Getters, filled with 99.999 Te powder and a mixture of Cs_2CrO_4 and 84% Zr–16% Al(ST 101) nonevaporable getter alloy, respectively. They are resistively heated by a current flow. The evaporation rate has been monitored by a quartz crystal microbalance.

The photocurrent was produced by an Oriel 100 W high-pressure Hg arc lamp, equipped with a condenser lens, a diaphragm, a dichroic mirror, a series of interference bandpass filters (253.7, 270, 297, 334, and 355 nm, with 10 nm bandpass) and a fused silica lens. The light intensity at the substrate position was measured by a calibrated Si photodiode. The photoemitted electrons were collected by a circular anode, polarized at +100 V with respect to the photocathode (grounded). No space charge current limitation has been observed.

During the fabrication process, the substrate was held at 120 °C by resistive indirect heating. First, we deposited 10 nm of Te at a rate of 1 nm/min. Then, the film was illuminated by the 253.7 nm radiation and Cs was deposited at a rate of 1 nm/min. The photocurrent gave us a real time control of the growth process, as shown in Fig. 1. At the end of the fabrication, the Cs source and the substrate heater were simultaneously switched off. The cooling rate was 6 °C/min.

The Auger emission was excited by an electron beam operating at 3 keV, 1 μA, over a 30 μm$\times$30 μm area. Auger spectra have been measured using a single pass cylindrical mirror analyzer operating at 0.6% relative resolution and in the first derivative mode (modulation voltage of 15 V peak-to-peak). The signal intensities have been converted to atomic fraction using suitable sensitivity factors.[9] Auger depth profiles (ADP) were achieved by an Ar^+ ion gun, operating at 1 keV, 30 μA/cm^2, rastered over a 2 mm$\times$2 mm area. Mo films (60 nm thick, as measured by Rutherford backscattering spectroscopy) evaporated by electron bombardment onto a Si(100) wafer have been profiled to estimate the sputtering rate, namely 3 nm/min.

XPS spectra have been collected by a Leybold LHS-12 subsystem, equipped with a concentric hemispherical analyzer (CHA) and a nonmonochromatized, Mg x-ray source, tilted by 45° with respect to the CHA axis. We found a good compromise among energy resolution, signal-to-noise ratio, and acquisition time by setting the spectral resolution (energy analyzer+photon) at 2.1 and 0.93 eV for the wide-range and high resolution spectra, respectively. We did a few experiments at two different collection angles, namely 22.5° (near-normal collection) and 70° (grazing collection), to intentionally change the information depth. We calculated the sensitivity factors for the Cs 3*d* 5/2, Te 3*d* 5/2, and O 1s subshells from (i) the atomic photoionization cross section;[10] (ii) asymmetry parameters;[10] and (iii) the inelastic mean free path.[11] They result in 4.4, 3.8, and 0.62, respectively.

III. THE FORMATION OF Cs_2Te PHOTOCATHODE

Figure 1 shows the quantum efficiency (QE) at 254 nm of a typical photocathode fabricated onto a Mo substrate, as a function of the Cs nominal thickness, i.e., the evaporation time multiplied by the evaporation rate as measured by the quartz microbalance. The abscissa does not indicate the actual film thickness, since the sticking coefficient of the Cs atoms onto the film is presumably less than one. The photocathode formation starts at (a), where the Cs vapor reacts onto the pure Te film, then proceeds through (b), (c), and (d) showing several characteristic and reproducible changes in the slope of the photocurrent curve, and finally in (e) a maximum in the photocurrent is reached and the fabrication is terminated. In Fig. 2 is shown a wide-range XPS spectrum of the completed photocathode; the main peaks correspond to Cs 3*d*, Te 3*d*, and O 1s photoemission lines and Cs and Te MNN Auger electrons. The O contamination level is less than 3%, while that of C (not shown) is below the detection limit of the XPS technique ($\approx$1%). The lack of signal from Mo points out that the substrate is completely covered by the

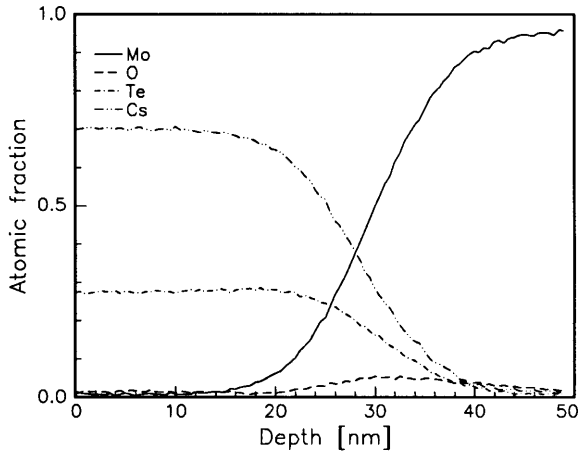

FIG. 3. Ar^+ Auger depth profile of the photocathode fabricated onto a Mo substrate.

photoemissive film, and diffusion of Mo from the substrate toward the surface of the film can be excluded.

The ADP shown in Fig. 3 rules out the presence of Mo up to 20 nm from the surface, and establishes the uniformity of the photoemissive film. The contamination from O is limited to the interface between the substrate and the film, and probably is due to a residual oxidized layer that survives to the substrate cleaning procedure. The width of the film/substrate interface is slightly larger than the depth resolution of the technique, therefore, an interfacial mixed-phase Mo–Cs–Te, roughly 5–10 nm thick, cannot be excluded, but the good operation of the photocathode is of no concerned, since it lays below the escape depth of the photoelectrons.

Photocathodes fabricated onto Cu substrates show a different ADP as shown in Fig. 4. The film composition is far from being uniform with depth, in that the large part of Cs is confined in the first 10 nm. A strong signal from the Cu substrate is always detectable, even at the very beginning of the erosion process, pointing out that the substrate material takes part in the photocathode formation. Alternatively, an island growth mechanism can explain the presence of Cu at

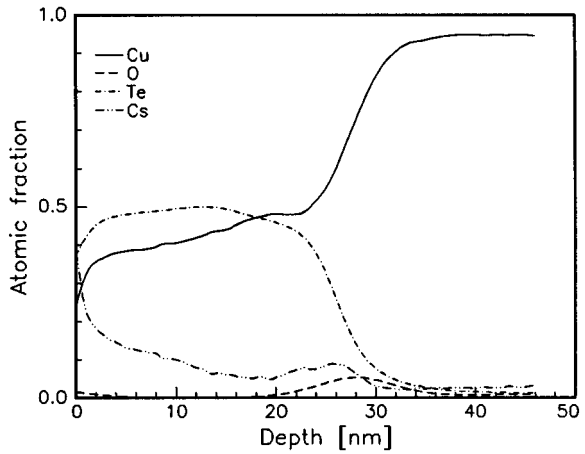

FIG. 4. Ar^+ Auger depth profile of the photocathode fabricated onto a Cu substrate.

TABLE I. Cs-to-Te ratio at the different fabrication steps of Fig. 1.

	Cs/Te	
	Normal	Grazing
Fig. 1(b)	0.6	···
Fig. 1(c)	1.2	···
Fig. 1(d)	1.9	1.8
Fig. 1(e)	2.5	2.4

the surface as an artifact of the ADP technique, but, at present, we are not able to settle this controversy. We did ''local'' Auger analysis by exploiting the scanning facility of our spectrometer, and we concluded that, if they exist, the islands must be less than 200 nm in diameter, i.e., the diameter of the primary electron beam. The relatively good QE (~4% at 266 nm) is a quite surprising value, but we have not analyzed thoroughly such photocathodes.

Let us return to the photocathodes fabricated onto Mo substrates. From XPS analysis (see Table I), the Cs-to-Te atomic fraction ratio is very similar in both near-normal and grazing collection, indicating that the film is homogeneous within the escape depth of the x-ray photoexcited electrons (≈2 nm). The Cs-to-Te ratio is 25% higher than what we expected on stoichiometric Cs_2Te, but this inconsistency could be due to the large uncertainty in the determination of the sensitivity factors.[12] If we are confident that the fabrication procedure produces stoichiometric Cs_2Te, then we could use it as a reference standard for the XPS line intensities to calculate the correct sensitivity factors for Cs and Te. On the other hand, we cannot exclude the presence of an excess of Cs in the photocathode. We regard the stoichiometry calculated on the basis of the sensitivity factors as a rough estimate of their ''true'' values, nevertheless, they are useful for semiquantitative considerations.

The ''stepped'' behavior of the QE vs the Cs nominal thickness of Fig. 1 suggests that the formation of the Cs_2Te film takes place through different phases. The Te 3*d* XPS features after each fabrication step are shown in Fig. 5. The spectra (b)–(d) have been synthesized in terms of three spectral components obtained by shifting and/or rescaling the spectrum of pure Te, curve (a), to minimize the sum of the squared residuals. The parameters of the peak synthesis are shown in Table II.

The synthesis procedure is justified by the charge potential model (CPM) for the core-level line shifts in photoemission.[12] The emitting atom is considered to be a hollow sphere on the surface of which the valence charge resides, while the neighboring atoms are considered simply as point charges. It is assumed that the binding energy (BE) shift of the photoemission lines is determined by the classical potential inside the sphere, the latter is easily expressed in terms of the valence charge on the emitting atom and a Madelung potential. CPM predicts equal shifts for all the core levels of an atom.

After 20 nm of Cs evaporation [Fig. 5(b)], a second Te component appears at 572.2÷572.3 eV, indicating that approximately a half of the Te reacts with the Cs vapor. The

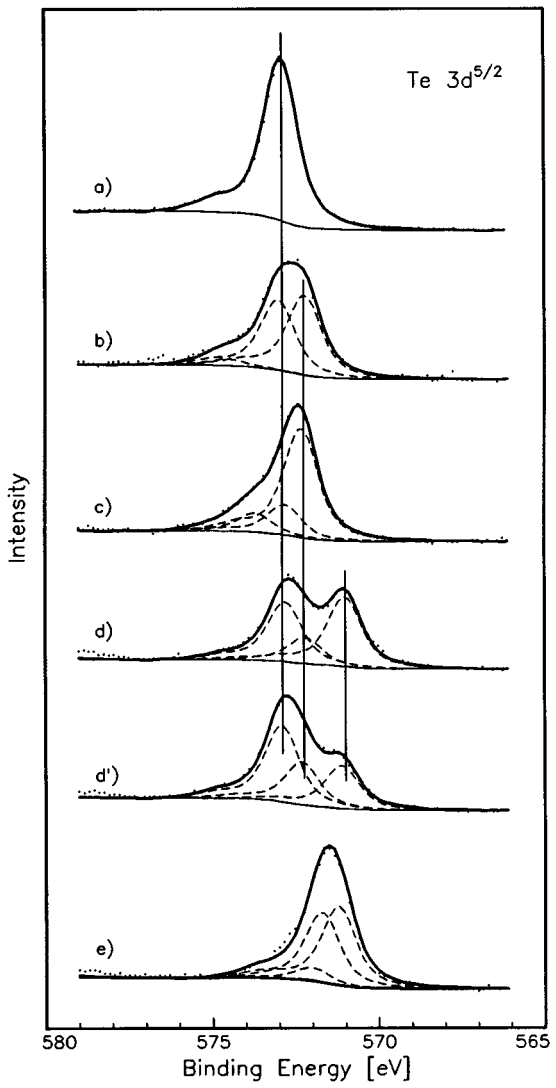

FIG. 5. Te $3d$ 5/2 line of the photocathode at the different fabrication steps. The labels refer to Fig. 1. Spectrum (d') has been measured at grazing collection geometry, all the others at near-normal collection. Spectra (b)–(e) have been synthesized in terms of the peak (a).

-0.6 to -0.7 eV BE shift, also indicates that a charge transfer from the Cs to the Te valence shells occurs. At this growth stage, the photocathode is in a two-phase state: ''pure,'' i.e., covalent, Te and a Cs–Te compound with a Cs-to-Te ratio of 1.2, as can be inferred from the data of Table I. As the Cs evaporation is carried on, the low BE component grows at the expense of the covalent Te one [Fig. 5(c)]. A small feature (12%) at $+0.8$ eV with respect to covalent Te can be observed.

At 60 nm of Cs deposition [Figs. 5(d) and 5(d′) at near-normal and grazing collection, respectively], the Te $3d$ line shape is synthesized by three components that have similar intensities: covalent Te at 572.9 eV, $Cs_{1.2}Te$ at 572.2–572.3 eV, and a new component at 571.0 ± 0.1 eV, which can be assigned to a Cs_xTe compound, with x higher than 1.2. The determination of the actual value of x from the data in Table I is difficult, because at this growth stage the film is not homogeneous within the escape depth of the Te $3d$ photoelectrons (2 and 0.7 nm at near-normal and grazing geometry), as pointed out by comparing the spectra taken in the two collection geometry. The intensity of Cs_xTe component reduces to 60% of its value when passing from near-normal to grazing collection, showing that the formation of that compound takes place approximately 5 nm below the surface.

The photocathode completion occurs after 70 nm of Cs deposition [Fig. 5(e)]. The quality of the peak synthesis is poorer with respect to the previous cases, indicating that the simple CPM model fails to explain the actual spectral shape. Nevertheless, the energy position of the barycenter of the full $3d$ feature (571.5 eV), is intermediate between $Cs_{1.2}Te$ and Cs_xTe. If we assume that phase(e) corresponds to Cs_2Te, then the Cs_xTe component, falling at a BE lower than that of Cs_2Te, should correspond to a Cs–Te compound with $x>2$.

In Fig. 6 are shown the spectral responses corresponding to the different growth steps indicated by the arrows in Fig. 1. As the Cs-to-Te ratio grows, the QE gets better at all wavelengths, but the increase is more marked in the low-energy part of the spectrum. When passing from 6(d) to 6(e),

TABLE II. Results of the peak synthesis of Figs. 5 and 9. The spectra of Fig. 5 have been decomposed in terms of spectral components obtained by shifting and/or rescaling the spectrum of Fig. 5(a), i.e., pure Te. For spectra of Fig. 9 we used as ''basic'' components pure Te and the line shape of the completed photocathode of Fig. 5(e).

	BE (eV)	Intensity (%)	BE (eV)	Intensity (%)	BE (eV)	Intensity (%)
Fig. 5(a)	Considered as a single component at 572.9 eV					
Fig. 5(b)	573.0	45	572.2	51	574.5	4
Fig. 5(c)	572.8	19	572.3	69	573.7	12
Fig. 5(d)	572.8	38	572.2	17	570.9	45
Fig. 5(d′)	572.9	47	572.3	26	571.1	27
Fig. 5(e)	571.2	49	571.7	43	572.6	8
Fig. 9(a)	Same as Fig. 5(e), but considered as a single component at 571.5 eV					
Fig. 9(b)	572.9	19	572.2	24	575.7[a]	57[a]
Fig. 9(c)	571.5[b]	65[b]	573.2	27	575–577[c]	8[c]

[a]Obtained by the difference between spectra of Fig. 9(b) and the two previous components.
[b]This component is the spectra of Fig. 5(e) without any energy shift.
[c]The energy position of these two components is not well defined; the indicated intensity is actually the sum of the two intensities.

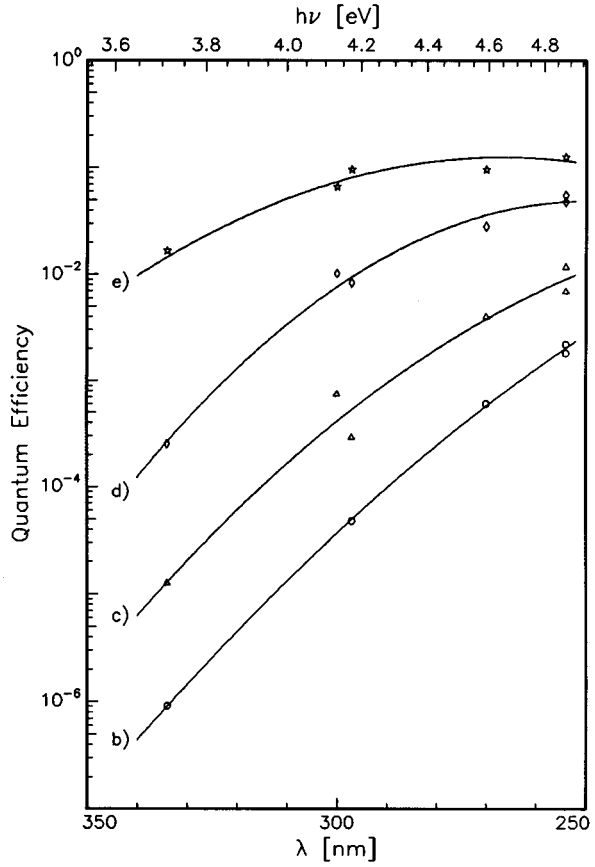

FIG. 6. Spectral response of the photocathode at the different fabrication steps. The labels refer to Fig. 1.

the QE increases two order of magnitudes at 334 nm (3.7 eV), while it approximately doubles at 254 nm (4.9 eV). In the frame of the three-step model,[13] such a large variation in the QE for a relatively small change in the photon energy, can be explained in terms of a reduction of the photoemission threshold caused by the reaction with Cs, and Fig. 5 indicates that this corresponds to the formation of the Cs_2Te compound. This strong enhancement of the QE at low-photon energies can be used during the fabrication as a ''warning light'' of the formation of the stoichiometric compound.

IV. POISONING

The operational lifetime of the Cs_2Te photocathode under the non-UHV conditions that normally occur in the rf cavities, has been tested by exposing it to few hundred langmuirs ($1\ L=10^{-6}$ Torr s) of different gases, namely, CO, N_2, CH_4, CO_2, and O_2. Their effect on the QE is shown in Fig. 7. 150 L of CO, N_2, and CH_4 have no consequence on the lifetime of photocathodes. CO_2 and O_2, on the other hand, have a poisoning effect that reduces the QE to $1/e$ with respect to its initial value after a 1100 and 15 L exposition, respectively. As concerns the poisoning with O_2, the QE shows a quite fast drop followed by a saturation, rather than an exponential decay law, indicating that a sort of surface passivation takes place. This behavior has been observed under more realistic vacuum conditions, i.e., during the operation of the photocathode in the rf cavity; the QE decreased roughly as a sequence of two exponential decays, the former lasts 30 h with a decay time of 21 h, the latter lasts 250 h and the decay time is 670 h.[14]

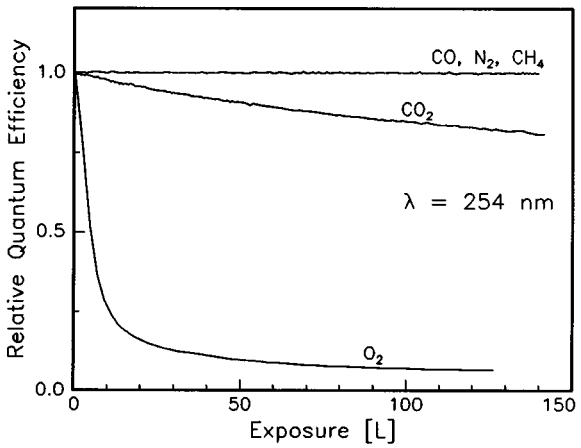

FIG. 7. Quantum efficiency drop for the 254 nm radiation of the photocathode exposed to different gases.

In Fig. 8 are shown the wide range XPS spectra of the photocathode before (a) and after a 120 L O_2 exposure [Figs. 8(b) and 8(b′)] at near-normal and grazing collection, respec-

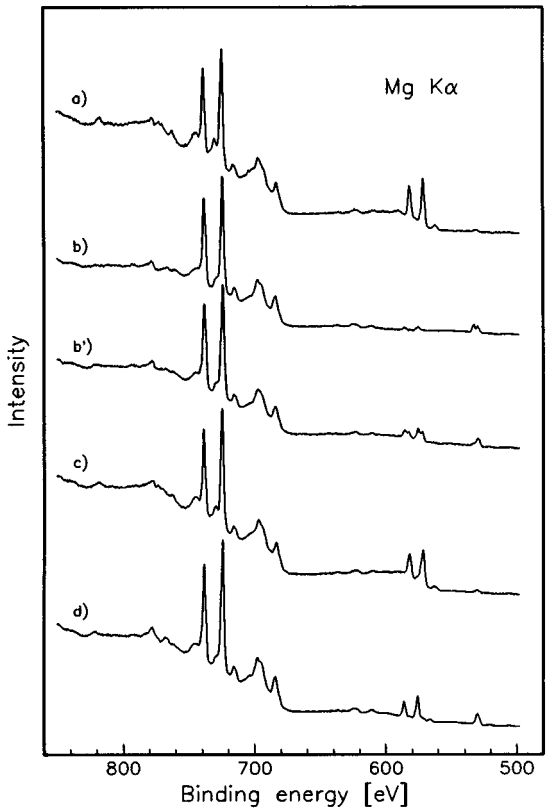

FIG. 8. Wide range XPS spectra from (a) the photocathode just after the fabrication; (b) after the 120 L O_2 exposition, at near-normal collection; (b′) same as (b), but at grazing collection; (c) after 1 h at 230 °C and under the effect of the 254 nm radiation; and (d) after 1 h at 230 °C without the 254 nm radiation.

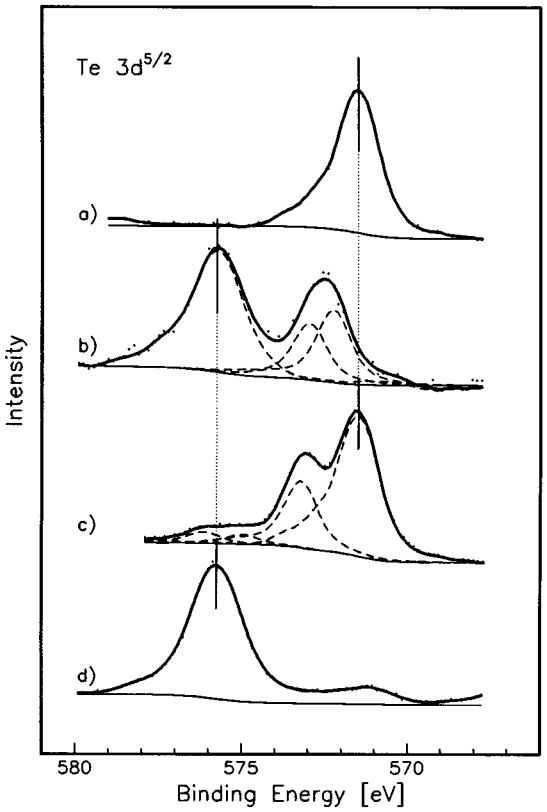

FIG. 9. The Te $3d^{5/2}$ photoemission line (a) from the photocathode just after the fabrication; (b) from the photocathode exposed to 120 L O_2, at grazing collection geometry; (c) after 1 h at 230 °C and under the effect of the 254 nm radiation; and (d) after 1 h at 230 °C without the 254 nm radiation. The photoemission lines have been synthesized in terms of the peak (a) and (e) of Fig. 5, namely pure Te and the completed photocathode, respectively.

tively. The Cs-to-Te ratio changes from 2.4–2.5 to 24 and 5.7 after the oxidation at near-normal and grazing collection, respectively, indicate that the Te content decreases as the depth increases. On the other hand, the Cs-to-O ratio is 1.4 and 1.7 at near-normal and grazing collection, respectively, suggesting that the O distribution is almost uniform along the escape depth of the photoelectrons. All these experimental data are consistent with the existence of approximately one monolayer of Te on the surface of a thick (thicker than the escape depth of the photoelectrons, ≈2 nm) Cs oxide layer.

The Te 3*d* peak at grazing collection is shown in Fig. 9(b). The low BE feature can be synthesized with two components at 572.9 and 572.2 eV, which have been identified as covalent Te and $Cs_{1.2}Te$, respectively. The Cs_2Te peak (571.5 eV) is completely suppressed by the oxidation process. The high BE peak indicates that approximately one half of the Te in the surface layer is in an oxidized state. On inspection of the angular dependence of the O 1s line [Figs. 10(a) and 10(a′)], we assign the 533.5 and the 530.2 eV components to the ''bulk'' and ''surface'' oxygen, respectively.

V. REJUVENATION

Cs_2Te photocathodes degraded by exposure to poor vacuum conditions could be rejuvenated by a heating

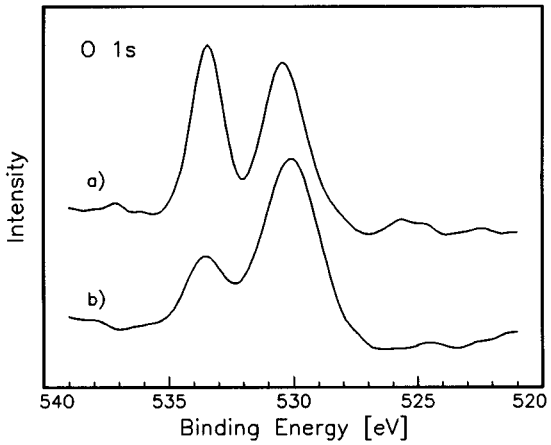

FIG. 10. The O 1s photoemission line from the oxidized photocathode (a) at near normal collection and (b) at grazing collection.

process.[4] We found that the effectiveness of this procedure depends on the fabrication procedure itself and on the lighting conditions during the heating process. In Fig. 11 is shown the QE dependence on heating time in three different situations. In each case, the substrate temperature was held to 230 °C. Curve (a) refers to a photocathode whose fabrication procedure was brought to the end [step (e) of Fig. 1]. The 254 nm uv radiation used to produce the photocurrent was incident continuously on the sample. After approximately one hour, the QE became stable at 30% of its value before oxidation, and a dull grey spot was visible in correspondence to the area that had been exposed to the uv radiation. Figure 8(c) shows that the photocathode rejuvenated under the effect of the uv radiation recovers the initial Cs-to-Te value of 2.5 and loses about 60% of the oxygen adsorbed during the poisoning process.

Figure 11(c) refers to the same experiment, but the average uv light power was reduced to 3% by a shutter. Actually, only the light strictly needed to monitor the process was

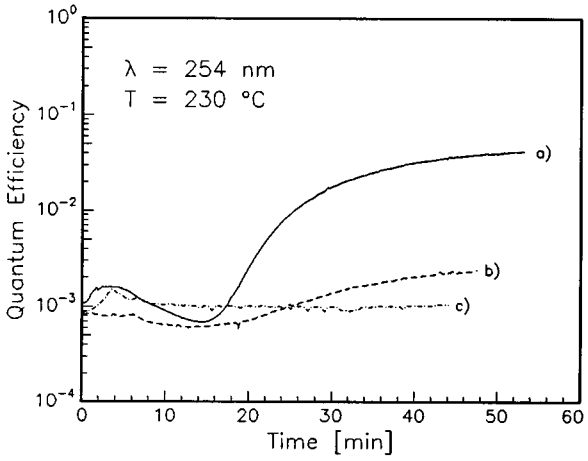

FIG. 11. Rejuvenation of the photocathodes exposed to 120 L O_2. The heating temperature is 230 °C and the 254 nm radiation was used to monitor the rejuvenation process. (a) completed photocathode [step (e) of Fig. 1]; (b) partially completed photocathode [step (d) of Fig. 1]; and (c) same as (a), but the uv light intensity was reduced to 3%.

shed onto the photocathode. In this case, no rejuvenation (and no dull grey spot) was observed after one hour, indicating that the uv radiation plays a role in the recovering mechanism. Furthermore, no oxygen was desorbed [Fig. 8(d)] and the correct Cs-to-Te value was not recovered, being 4.4 instead of 2.5.

The result of the combined effect of uv radiation and temperature on a partially completed photocathode [step (d) of Fig. 1], which has been subsequently oxidized in the same way as the previous one was, is shown in curve (b) of Fig. 11. The behavior is similar to that of curve (a), but the QE gain is considerably reduced. Rejuvenation is, thus, a property that belongs to Cs_2Te and not to its ''precursor'' compound, namely the $Cs_{x>2}Te$ of Figs. 5(d) and 5(d′).

The Te 3*d* XPS line of the completed photocathode, rejuvenated under the effect of the uv radiation is shown in Fig. 9(c). About 70% of the peak is represented by Te in the Cs_2Te form (571.5 eV), again indicating the effectiveness of the rejuvenation process. Almost all of the remaining 30% falls at 573.2 eV BE. Thus, it is in a chemical state close to that of covalent Te. Traces of Te oxide(s) are visible in the ≈576 eV region. On the contrary, the rejuvenation process under the effect of the temperature alone, leads to a Te 3*d* line that is completely synthesized by the Te oxide(s) component, as shown in Fig. 9(d).

VI. CONCLUSIONS

Thin films of Cs_2Te photocathodes have been fabricated, transferred, and analyzed by Auger and XPS spectroscopy under UHV conditions. Cu and Mo substrates have been employed, giving high QE values (6% and 12%, respectively). Strong contamination from the substrate material has been observed in photocathodes fabricated onto Cu, and the film structure is far from being uniform. As far as the photocathodes fabricated onto Mo are concerned, the Cs_2Te formation goes on through several steps: (i) a two-phases system $Te+Cs_{1.2}Te$ is observed at the beginning of the reaction of the Te film with the Cs vapor; (ii) as the Cs deposition is carried on a new $Cs_{x>2}Te$ phase has been detected ≈0.5 nm below the surface; (iii) finally, a homogeneous, single phase Cs_2Te film results.

The lifetime of the photocathodes exposed to different gases, namely, O_2, CO_2, CO, N_2, and CH_4, has been measured. The oxidation of the photocathode quickly reduces the QE and the photocathode develops a thick layer of caesium oxide at the surface.

The oxygen damages could be partially recovered by heating the photocathode to 230 °C under the effect of the 254 nm uv radiation. No rejuvenation has been observed under the effect of the temperature alone.

ACKNOWLEDGMENT

This work was partially supported by the Human Capital and Mobility Contract No. ERB CHRX CT 940455, titled ''High Current Photoemission and Bright Injectors.''

[1] A. H. Sommer, *Photoemissive Materials* (Wiley, New York, 1968).
[2] R. A. Powell, W. E. Spicer, G. B. Fisher, and P. Gregory, Phys. Rev. B **8**, 3987 (1973).
[3] E. Chevallay, J. Durand, S. Hutchins, G. Suberlucq, and M. Wurgel, Nucl. Instrum. Methods A **340**, 146 (1994).
[4] S. H. Kong, J. Kinross-Wright, D. C. Nguyen, and R. L. Sheffield, J. Appl. Phys. **77**, 6031 (1995); S. H. Kong, D. C. Nguyen, R. L. Sheffield, and B. A. Sherwood, Nucl. Instrum. Methods A **358**, 276 (1995).
[5] R. L. Sheffield, E. R. Gray, and J. S. Fraser, Nucl. Instrum. Methods A **272**, 222 (1988).
[6] A. Michalke, H. Piel, C. K. Sinclair, and P. Michelato, in *Proceedings of the Third European Particle Accelerator Conference* (Frontiers, Gif-sur-Yvette, France, 1992), Vol. 2, p. 1014.
[7] P. Michelato, P. Gallina, and C. Pagani, Nucl. Instrum. Methods A **340**, 176 (1994).
[8] S. Valeri *et al.*, in *Proceedings of the Fourth European Particle Accelerator Conference* (World Scientific, Singapore, 1994), Vol. 2, p. 1459.
[9] L. E. Davis, N. C. MacDonald, P. W. Palmberg, G. E. Riach, and R. E. Weber, *Handbook of Auger Electron Spectroscopy* (Physical Electronics, Eden Praire, MN, 1978).
[10] J. J. Yeh and I. Lindau, At. Data Nucl. Data Tables **32**, 1 (1985).
[11] M. P. Seah and W. A. Dench, Surf. Interface Anal. **1**, 2 (1979).
[12] D. Briggs and J. C. Rivière, in *Practical Surface Analysis*, edited by D. Briggs and M. P. Seah (Wiley, Chichester, England, 1990), Vol. 1, p. 85.
[13] W. E. Spicer, Phys. Rev. B **112**, 114 (1958).
[14] H. Braun, J. P. Delahaye, and I. Wilson, The CLIC Test Facilities, CERN CLIC Note 293.